Superfluidity and mean-field energy loops: Hysteretic behavior in Bose-Einstein condensates

Erich J. Mueller*
Department of Physics, The Ohio State University, Columbus, Ohio 43210
(Received 2 September 2002; published 16 December 2002)

We present a theory of hysteretic phenomena in Bose gases, using superfluidity in one-dimensional rings and in optical lattices as primary examples. Through this study we are able to give a physical interpretation of swallow-tail loops recently found by many authors in the mean-field energy structure of trapped atomic gases. These loops are a generic sign of hysteresis, and in the present context are an indication of superfluidity. We have also calculated the rate of decay of metastable current-carrying states due to quantum fluctuations.

DOI: 10.1103/PhysRevA.66.063603 PACS number(s): 03.75.Fi

I. INTRODUCTION

Quantum degenerate bosonic atoms have proven important for studying macroscopic quantum phenomena (for a review see Ref. [1]). The order parameter of the condensed phase is a macroscopic quantum wave function which, unlike single-particle wave functions, can be directly probed in an experiment. The interplay between this macroscopic wave function and interactions leads to a variety of effects, the most well known of which is superfluidity. Here we explore superfluid phenomena in a dilute atomic gas with short-range interactions. As we will show, *superfluidity is naturally viewed as a hysteretic response to rotation*, motivating a more general study of hysteresis.

In our study of superfluidity, we quantify the roles played by interactions, finite-size effects, and impurities in the behavior of a weakly interacting gas of one-dimensional Bosons, showing that persistent currents can exist when the interactions are strong compared to any impurity potentials, but weak enough to not produce large phase fluctuations. We present a detailed discussion of the energy landscape of such gases, revealing a nontrivial topography. In the limit of weak interactions we calculate the lifetimes of persistent currents.

In addition to gaining insights into superfluidity within a one-dimensional geometry, our approach provides an intuitive understanding of *swallow-tail energy loops* found in mean-field studies of Bose gases within periodic potentials [2–5]. We show that such loops are a generic feature of hysteresis and, in the case of atoms in a periodic potential, the loops are a manifestation of superfluidity. We discuss the underlying quantum scaffolding that supports this mean-field structure, and identify other settings where it can be observed.

In Sec. I A we introduce the basic phenomenon of hysteresis. The remainder of this section discusses superfluidity and provides examples of scenarios in which a Bose-Einstein condensate will behave hysteretically. Section II discusses microscopic models for superfluidity in both a ring-shaped geometry and in an optical lattice. The remainder of this paper analyzes these models.

A. Generic properties of hysteresis

Hysteresis is the phenomenon where the state of a physical system depends upon its history. The canonical example is a ferromagnet, which in zero applied magnetic field has a spontaneous magnetization, conventionally taken to be in the $\hat{z}$ direction. This magnetization is robust in that it is not significantly changed applying a small field in the $-\hat{z}$ direction. However, if a strong enough field is applied, the magnetization can ''flip,'' and point in the $-\hat{z}$ direction. When the applied field is reduced to zero, the magnetization does not revert to its original orientation, but remains pointing in the $-\hat{z}$ direction. In this example, and the ones that follow, we see that the response of the system lags behind the applied stimulus.

In a classical system, hysteresis is conveniently thought about in analogy to the Landau theory of phase transitions [6]. One considers the property of interest (in this case the magnetization M) to be an order parameter. An energy landscape is produced by calculating the energy of the system as a function of this order parameter. The applied field (here the magnetic field H) changes this landscape.

Hysteresis occurs when the energy landscape has more than one minimum, as depicted in Fig. 1(a) (for similar figures calculated within a microscopic model, see Figs. 12 and 13). For example, both magnetization in the $\hat{z}$ and $-\hat{z}$ directions might be local minima. Applying a field tilts the landscape, and reduces the barrier. At some critical field, the barrier disappears and the system jumps into the global minimum [Figs. 1(b) and 1(c)]. The phenomenon where the barrier disappears goes under several names; in the theories of

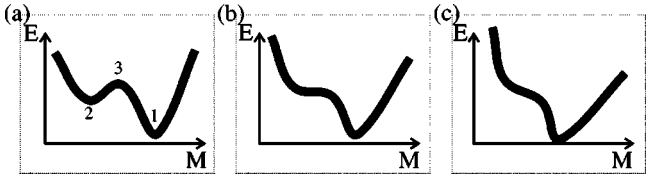

FIG. 1. Typical energy landscapes: energy E vs order parameter M. In (a) two minima (labeled 1 and 2) are separated by a barrier (3). In (b) one minimum and the barrier coalesce. In (c) only one minima exists. A control parameter (H) tunes from one landscape to another. A plot of the energy of the extrema versus the control parameter is shown in Fig. 2.

*Electronic address: emueller@mps.ohio-state.edu

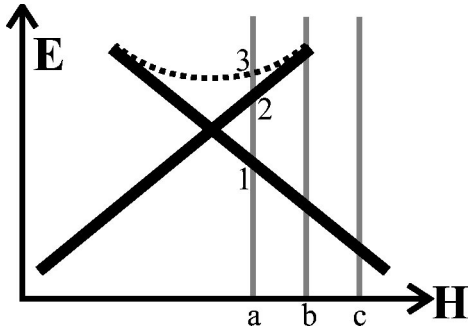

FIG. 2. Energy extrema as a function of control parameter H. Solid lines denote minima, dotted line denotes maxima/saddles. The points labeled a, b, and c coincide with the energy landscapes in Fig. 1, which, respectively, have 3, 2, and 1 extrema. The points labeled 1, 2, and 3, coincide with the same points in Fig. 1(a). The existence of multiple minima at the same value of the control parameter is a ubiquitous sign of hysteresis. The presence of two minima requires a maximum/saddle (see Fig. 1).

phase transitions [6] and of gradient dynamics [7] it is, respectively, known as a spinodal or a catastrophe. In more mathematical treatments it is referred to as a ''saddle-node bifurcation.''

Figure 2 gives a generic depiction of the energy of the extrema of the energy landscape (again, similar figures calculated from microscopic models are shown in Fig. 11). A distinctive loop is seen. This loop, referred to as a ''swallow tail'' by Diakonov *et al.* [3], is a general feature of the spectrum of a hysteretic system. It exists because for some range of fields there are three extrema (two local minima and a maximum). At the point labeled by (c), one of the local minima meets up with the maximum, and they annihilate one another.

To better match the dynamical systems literature, it would be preferable to not refer to Fig. 2 as a swallow tail, and instead reserve the term for the similar structure in Fig. 3 that

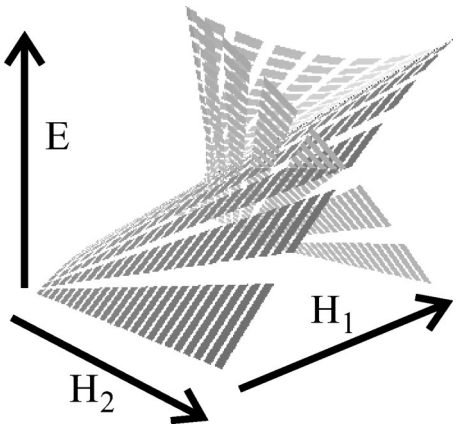

FIG. 3. Three-dimensional depiction of a swallow-tail energy structure. The x and y axes represent control parameters, here referred to as H_1 and H_2, while the vertical axis is the energy E. The self-intersecting surface shows the stationary points of the energy. A two-dimensional slice is seen in Fig. 2 where H_1 can be identified with H.

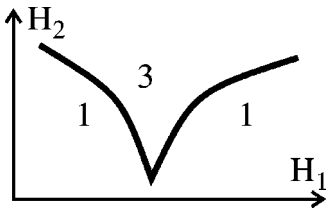

FIG. 4. Catastrophe set: values of control parameters for which the number of extrema of the energy structure in Fig. 3 change. Inside the cusp there are three extrema (two minima and a maximum) while outside there is only one.

occurs when one has two control parameters. The second control parameter changes the size of the loop, and can be tuned so that the loop, and all hysteresis, vanishes. A model that gives rise to this latter structure will be discussed later.

A possible point of confusion here is that the term ''swallow tail'' is traditionally used to discuss not the energy structure, but rather the catastrophe set, which is the points (in the control parameter space) where the number of extrema in the energy landscape change. The catastrophe set corresponding to Figs. 2 and 3, respectively, consists of two points and the cusplike structure in Fig. 4. Thus the swallow-tail energy spectrum is associated with a *cusp catastrophe* and not a *swallow-tail catastrophe*.

The local minima in the energy landscape are of great physical importance, as the system typically resides in their vicinity. Saddle points, and local maxima, are also important in that the rate of transitions from one minima to another are governed by the lowest barrier separating the minima. In classical systems, these transitions are typically caused by thermal fluctuations, and occur at a rate proportional to e^{-E_b/k_bT}, where E_b is the barrier height, k_b is the Boltzmann's constant, and T is the temperature. It should be noted that only in very rare physical situations does the system spend much time at one of these extrema.

In a quantum-mechanical system the scenario for hysteresis that we have discussed becomes more complicated. The basic difficulty is that the order parameter is generally not a constant of motion. In this case one does not know how to answer questions like ''what is the energy of the system when the magnetization points in the $+\hat{z}$ direction?'' There may simply not exist any energy eigenstates for which the magnetization points in that direction. Consequently, it is by no means obvious how to construct an energy landscape, and what significance it will have.

There are three, roughly equivalent, methods of circumventing this difficulty. The first approach is to write the Hamiltonian as a sum of two terms, $H=H_{\mathrm{diag}}+H'$, where the order parameter commutes with H_{diag}. This diagonal term is the projection of the Hamiltonian into the space where the order parameter has a definite value. For example, if we have a spin system where the z component of the magnetization is our order parameter, then H_{diag} would be diagonal in a basis $\{|S,S_z\rangle\}$, where S is the total spin, and S_z is the projection of the spin along the z axis. If H' is small, one can neglect it for the sake of drawing the energy landscape. The second approach is to use a variational scheme, where one writes ''reasonable'' wave functions that are param-

etrized by the order parameter. The expectation value of the energy in these states is an approximation to the energy landscape. The final approach is to use a mean-field theory in which the order parameter is a constant of motion. This discussion will be more concrete once microscopic models are introduced in Sec. II and used to produce energy landscapes.

All three of these schemes share the feature that if the system starts in a local minimum of the energy landscape, there can be matrix elements in the original Hamiltonian which allow the system to tunnel to another minimum. This procedure can be thought of in analogy to classical thermally activated transport, where due to thermal fluctuations the system can jump from one minimum to another. Here it is quantum fluctuations that allow the system to move between minima.

B. Superfluidity

We now turn to a discussion of superfluidity, a phenomenon that manifests itself in many related ways, including, dissipationless flow, quantized vortices, reductions in the moment of inertia, and the existence of persistent currents. We focus on the latter phenomenon, which was first observed in ^{4}He [8]. In an idealized version of these experiments, an annular container of helium is rotated while cooling to below the lambda temperature, where it becomes a superfluid. When the container is then stopped, one observes that the fluid continues to rotate—maintaining its velocity for extremely long times. Arguments based solely on Galilean invariance show that this current-carrying state cannot be the ground state of the system, and is therefore an extremely long-lived metastable excited state [9]. It is observed that the lifetime of these currents decrease with increasing velocity, and there is a critical velocity v_c, above which no persistent currents exist.

For our purposes it is convenient to think of such currents in terms of a hysteretic response to rotation. Imagine starting with an annular container of superfluid which is at rest. If the container is slowly rotated in a clockwise direction the fluid remains at rest (in the rotating frame this is a persistent current). If one rotates faster and faster, the relative velocity between the container and the fluid eventually exceeds the critical velocity, excitations are formed, and the fluid accelerates. At this point, a persistent current has developed in that even if one stops rotating the container then the fluid will continue to flow. The flow can be stopped if one rotates the container sufficiently fast in a counterclockwise direction. The principle is simply that when the relative velocity between the fluid and the container exceeds v_c, the fluid accelerates. Thus the fluid flow lags behind the applied rotation, resulting in the hysteresis loop sketched in Fig. 5. By the arguments of Sec. I A, one must therefore see energy structures analogous to those in Figs. 1 and 2.

Here we wish to understand the origin of this dramatic effect from a microscopic model. Standard descriptions of superfluidity [6,10] attribute the long life of these currents to the scarcity of low-energy excitations. In the present setting, it is more natural to think of superfluidity in terms of the ability of the fluid to screen out impurities. The basic argument, which will be given in more detail later, is that an ordinary (nonsuper) fluid does not support persistent currents because the fluid particles scatter off of small imperfections in the walls of the container, exchanging angular momentum and eventually equilibrating with those walls. Through a collective deformation of the macroscopic wave function, quantum degenerate bosons are able to screen out the imperfections. Since the fluid effectively sees smooth walls, it does not slow down. In the body of this paper, these imperfections will be modeled as an ''impurity'' potential.

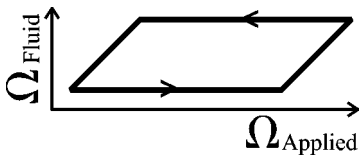

FIG. 5. Hysteresis loop in a superfluid. The rotation rate of the fluid is shown as a function of the rotation of the container. The arrows denote the direction of the hysteresis loop. As seen in experiments on helium [8], the sloped lines are actually made up of many discrete jumps, which cannot be resolved on this scale.

From this physical picture, one can anticipate many of our results. In particular, there are two natural control parameters, the rate of rotation and the strength of interactions relative to the impurity potential. We will find an energy structure similar to Fig. 3, where these two control parameters correspond to H_2 and H_1.

C. Optical lattices

Superfluidity is not limited to a ring geometry. As we explain, superfluid properties naturally appear for Bose particles within a periodic potential. Due to their importance in solid-state physics, quantum phenomena in periodic potentials are very well studied theoretically and there has been a rapid progress on experimental studies of Bosons in periodic potentials, where the periodicity is produced using standing waves of light (optical lattices) (for a review see Ref. [11]). Many of the single-particle phenomena of solid-state physics have been observed in these artificial lattices, including band structure, Bloch oscillations, and Zener tunneling [11]. These solid-state concepts are reviewed below, and play an important role in our discussion of superfluidity. Further theoretical discussions of these phenomena in cold gases and relevant discussion of how interactions screen the lattice can be found in Ref. [12]. Although not directly related to our study of hysteresis, it is worth mentioning that correlated many-body states, such as Mott insulators [13], have been observed in atoms trapped in an optical lattice.

Here we use superfluidity to reexamine theoretical studies of mean-field energy loops of atoms in optical lattices [2,3]. We understand the key features of these studies by starting with the energy structure of the noninteracting single-particle states. As discussed in Ref. [14], the states available to noninteracting particles in a periodic potential are labeled by two quantum numbers, a band index ν, and a *crystal momentum* k. The wave functions of these states are of the Bloch form,

$$\psi_{\nu k}(r) = e^{ikr} v_{\nu}(r), \tag{1}$$

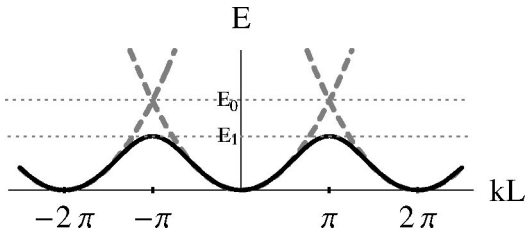

FIG. 6. Band structure. The solid line shows the energy of Bloch waves of crystal momentum k for noninteracting particles in a periodic potential within an extended zone scheme. The bandwidth, E_1, becomes smaller as the periodic potential becomes stronger. The dashed lines show the energy states in the absence of the periodic potential. At the band edge, these states have energy $E_0 = \hbar^2\pi^2/2mL^2$.

were $v_\nu(r)$ shares the periodicity of the lattice, and k is restricted to the first Brillouin zone. Limiting our discussion to one dimension with lattice periodicity L, the first Brillouin zone corresponds to momenta $|k| < \pi/L$. For simplicity, we use dimensionless units where $L=1$. In Fig. 6, the lowest-energy band is sketched in an extended zone scheme, where the energy is extended periodically to k's outside of the first Brillouin zone. This periodicity is the source of the phenomenon known as Bloch oscillations. Imagine starting with a single particle in the $k=0$ state. If an external force is applied to the particle, it will accelerate and k will increase. For sufficiently weak acceleration, the state will adiabatically follow the solid curve in Fig. 6. When k has increased to 2π, the system has returned to its initial state. Thus a constant force leads to periodic oscillations. If the force is too strong, the adiabaticity condition is violated, transitions are made to higher bands, and one no longer sees the Bloch oscillations. This breakdown is known as Zener tunneling.

A similar scenario can be considered for Bose condensed atoms. In the ground state all of the particles reside in the lowest-energy Bloch state. Like the single-particle case, when a force is applied, the crystal momentum k increases. However, as a superfluid, the condensate is able to screen out the periodic potential. Thus, for sufficiently strong interactions, instead of following the solid curve in Fig. 6, the system follows a path closer to the dashed curve, corresponding to the spectrum of states in the absence of the periodic potential. The microscopic model which will be introduced in Sec. II B confirms this picture, and one can identify the set of states visited during this adiabatic acceleration as local minima in a mean-field energy landscape. When the fluid's velocity exceeds the critical velocity, it loses the ability to screen the lattice. Thus the energy curves terminate at some point, and energy extrema take on the structure in Fig. 7, where one has a crossing of local minima. One minimum corresponds to the fluid moving to the right, the other to fluid moving to the left. These two states have different momentum, but share the same crystal momentum. For purely topological reasons, the presence of two local minima at a given value of k guarantees that there is a saddle point separating them. This barrier state is also shown in Fig. 7 as the dotted line forming the ''top of the swallow's tail.'' As will be discussed in Sec. III B, the barrier state corresponds to a ''phase slip.''

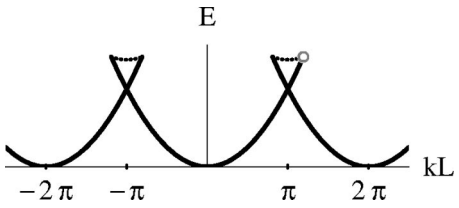

FIG. 7. Schematic representation of energy extrema for a condensate in an optical lattice. Solid and dotted lines denote minima and saddle points. One of the spinodal points, where the number of extrema change, is marked by a gray circle.

The question of what happens to the system when the cloud is accelerated past the ''end of the loop'' (marked by a gray circle on the figure) is discussed by Wu *et al.* [2,15] and Liu *et al.* [5]. Clearly adiabaticity must break down at this point, and crossing this point from left to right, then back again will not return the system to its original state. This irreversibility shows that hysteresis has developed.

Note that as the interaction strength is reduced, the loops in Fig. 7 become smaller and eventually disappear. Thus if one identifies H_1 with k and H_2 with the interaction strength, the mean-field energy extrema near $k=\pi$ must have the full swallow-tail structure shown in Fig. 3.

D. Josephson junctions

We conclude the introduction by discussing a hysteretic Bose system in which the hysteresis is not associated with persistent currents, namely, a gas of particles with attractive interactions in a double-well trap as depicted in Fig. 8. The control parameters here are the strength of interactions and the bias δ that is applied between the two wells.

Figure 9 illustrates the transformations that give rise to a hysteresis loop in this system. One starts with the left well of much lower energy than the right ($\delta>0$). The ground state consists of all of the particles bunched up on the left. The bias is then slowly decreased, and made slightly negative, so that the right-hand well has lower energy. In the true ground state all of the particles are sitting in the right-hand well. Nonetheless, the particles actually stay in the left-hand well. This behavior is understood by noting that in order to move the particles from the left-hand well to the right, one has to first move a single particle. Although such a move saves the potential energy of the bias, separating that one particle from

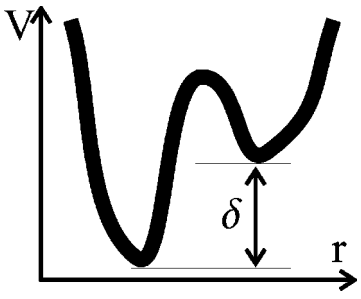

FIG. 8. Geometry of a double-well trap. The potential energy V is shown as a function of a spatial coordinate r. The two wells have an energy difference δ.

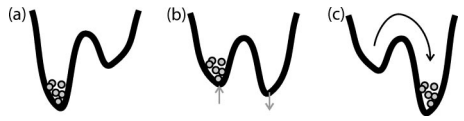

FIG. 9. Illustration of hysteresis in a double-well trap filled with attractive bosons. In each picture the trap from Fig. 8 is shown with a set value of δ, and the particles shown by small gray circles in one of the two wells. In (a) the bias is positive, and all of the particles are in the left well. The bias is slowly switched to a small negative value in (b). The particles remain in the left-hand well, even though the ground state has all of them on the right. For large enough negative detuning (c), the particles all jump to the right.

the others makes the interaction energy less negative. For small enough bias, moving a single particle increases the total energy, and the state with all of the particles sitting in the left-hand well is a local minimum of the energy. If the bias is made more negative, the potential energy savings of moving a particle to the right-hand side eventually becomes greater than the interaction energy cost. The particles then all jump to the right-hand well. The whole process can be reversed, and a hysteresis loop is formed.

For weaker interactions, the value of δ at which the metastable state disappears becomes smaller. For sufficiently weak interactions, no hysteresis occurs. Thus identifying H_2 with the interaction strength, and H_1 with the detuning δ, the energy landscape has extrema matching Fig. 3.

Experimentally, such a double-well trap can be formed by considering two cells in an optical lattice, or by carefully arranging magnetic and optical fields as in Ref. [16]. We will not explicitly discuss models for this system, as there exist many excellent treatments in the literature [17].

II. MICROSCOPIC MODELS

We now construct microscopic models of the superfluid systems described in the Introduction. In addition to verifying the qualitative structures already discussed, these models allow us to make quantitative predictions about the behavior of a gas of bosons. In particular, as mentioned in Sec. I A, a quantum-mechanical system can tunnel from one minimum in the energy landscape to another (which would, for example, lead to the decay of persistent currents). We are able to calculate the rate of such tunneling.

A. Superfluidity

As a microscopic model of persistent currents, we study a one-dimensional ring of length L, rotating at frequency Ω, containing a cloud of bosons of mass m which interact via short-range interactions. Measuring energy in terms of $\hbar^2/2mL^2$ ($\hbar$ is Planck's constant), the Hamiltonian in the rotating frame is

$$H=\sum_j (2\pi j+\Phi)^2 c_j^\dagger c_j+(g/2)\sum_{j+k=l+m} c_j^\dagger c_k^\dagger c_l c_m, \quad (2)$$

where $\Phi=2mL^2\Omega/\hbar$ and $g>0$ are dimensionless measures of the rotation speed and the strength of the interactions. Operators $c_j^\dagger$ create bosons with angular momentum $j\hbar$. The model (2) could be experimentally realized by cooling an atomic gas in an annular trap with harmonic confinement of frequency $\omega_\perp$ to such an extent that only the lowest transverse mode is occupied (for recent experimental progress on annular traps see Ref. [18]). As long as the trap length $d_\perp=\sqrt{\hbar/m\omega_\perp}$ is larger than the scattering length a_s the interaction parameter would then be given by $g=4\pi a_s L/d_\perp^2$.

Despite its apparent simplicity, this one-dimensional model is quite rich. It is a canonical example of a Luttinger liquid [19] whose behavior can be studied via the Bethe ansatz [20]. Two properties worth noting are: 1) at $g=0$ it describes a noninteracting Bose gas; and 2) at $g\to\infty$ it can be mapped onto a gas of noninteracting fermions. In neither of these limits is the system superfluid, however, we show that for small positive g the system *is* superfluid. Here we will study how this superfluidity develops as g is tuned from 0, finding the structure discussed in Sec. I B. The equally interesting question of how this superfluidity breaks down as $g\to\infty$ will not be discussed.

The model Hamiltonian (2) is invariant under rotation, and therefore conserves angular momentum. A trivial consequence is that if a current is started in this system it will never decay. Thus, as aptly pointed out by Kagan *et al.* [21], to study superfluidity one must add an impurity that breaks the symmetry. In an experimental setting such terms are always present due to imperfections in the apparatus. It is quite instructive to imagine artificially introducing such an impurity (for instance, by using a laser that interacts with the atoms via dipole forces), and being able to control its strength. Conventional discussions of superfluidity focus on ^{4}He, which is strongly interacting, and whose behavior is largely insensitive to the strength of the impurities. In a weakly interacting setting (especially in one dimension) this is no longer the case, and the strength of the symmetry-breaking term is extremely important. The system's behavior is relatively insensitive to the exact form of the impurity. Two natural models are a point scatterer $H_{\rm pnt}=\lambda\Sigma_{kq}c_k^\dagger c_q$ and a sinusoidal potential $H_{\rm sin}=\lambda\Sigma_k(c_k^\dagger c_{k-1}+c_k^\dagger c_{k+1})$. In both cases λ measures the strength of the perturbation.

B. Optical lattices

A model for particles in a periodic potential can be constructed which has the same structure as Eq. (2) with an impurity. The rotation speed Φ and the impurity potential are, respectively, mapped onto the crystal momentum and the lattice potential.

Introducing the field operator $\psi(x)$, which annihilates a particle at position x, the Hamiltonian for particles in one dimension interacting with a local interaction is

$$H=\int dx\,\frac{\hbar^2\nabla\psi^\dagger\cdot\nabla\psi}{2m}+V(x)\psi^\dagger\psi+\frac{\bar{g}}{2}\psi^\dagger\psi^\dagger\psi\psi, \quad (3)$$

where $V(x)$ is the lattice potential, $\bar{g}$ parametrizes the interactions, and the argument x is assumed for each of the field

operators. The periodic potential can be written as $V(x) = \Sigma_j e^{ip_j x} V_j$, where $p_j = jk_L = 2\pi j/L$ are reciprocal lattice vectors.

In analogy to Eq. (1), it is convenient to write our field operators in a Bloch form,

$$\psi(x) = \sum_j e^{ip_j x} \int_{-\pi}^{\pi} \frac{dk}{\sqrt{2\pi L}} e^{ikx/L} \psi_j(k), \tag{4}$$

where $\psi_j(k)$ is the Bose operator which annihilates a particle with momentum $\hbar(k+2\pi j)/L$. These obey the standard commutation relationships $[\psi_j(k), \psi_{j'}^\dagger(k')] = \delta_{jj'}\delta(k-k')$. In this decomposition, k is the (dimensionless) crystal momentum that runs from $-\pi$ to π and p_j are reciprocal lattice vectors. The index j plays the role of a band index in the limit that the lattice potential vanishes.

In terms of these operators, the Hamiltonian takes the form

$$H = \frac{\hbar^2}{2mL^2}(H_{\rm kin} + H_{\rm pot} + H_{\rm int}^{\rm (vert)} + H'_{\rm int}), \tag{5}$$

$$H_{\rm kin} = \int dk \sum_j (2\pi j + k)^2 \psi_j^\dagger \psi_j, \tag{6}$$

$$H_{\rm pot} = \int dk \sum_{jq} V_q \psi_{j+q}^\dagger \psi'_j, \tag{7}$$

$$H_{\rm int}^{\rm (vert)} = \int dk (g/2) \sum_{j_1 + j_2 = j_3 + j_4} \psi_{j_1}^\dagger \psi_{j_2}^\dagger \psi_{j_3} \psi_{j_4}, \tag{8}$$

$$H'_{\rm int} = \int d\{k\} (g/2) \sum_{\{j\}} \psi_1^\dagger \psi_2^\dagger \psi_3 \psi_4, \tag{9}$$

where the respective terms in Eq. (5) represent kinetic, potential, and interaction energy. The interaction is split into two terms, one $H_{\rm int}^{\rm (vert)}$ only involves particles with the same crystal momentum, while $H'_{\rm int}$ involves particles with different crystal momentum. In Eqs. (6) through (8) the argument k in $\psi_j(k)$ is omitted. In Eq. (9) the sum and integral are taken over all k_i, j_i such that momentum is conserved

$$k_1 + k_2 - k_3 - k_4 + 2\pi(j_1 + j_2 - j_3 - j_4) = 0, \tag{10}$$

and where not all of the k_i are equal. In Eq. (9) the shorthand notation $\psi_i = \psi_{j_i}(k_i)$ is used. The interaction is given by $g = \bar{g}/2\pi L$.

The meaning of each of these terms is illustrated in Fig. 10. Solid lines show the kinetic energy of free particles as a function of the crystal momentum k. The periodic potential conserves the crystal momentum and therefore only induces vertical transitions. The main effect of $H_{\rm pot}$ is therefore to split the degeneracies at the level crossings, giving rise to the band structure shown in gray. The two interaction terms scatter particles between these states. The ''vertical'' interaction $H_{\rm int}^{\rm (vert)}$ only involves particles that all share the same crystal momentum, as illustrated on the right side of Fig. 10(b). All other scattering processes, such as the one on the left side of Fig. 10(b) are included in $H'_{\rm int}$.

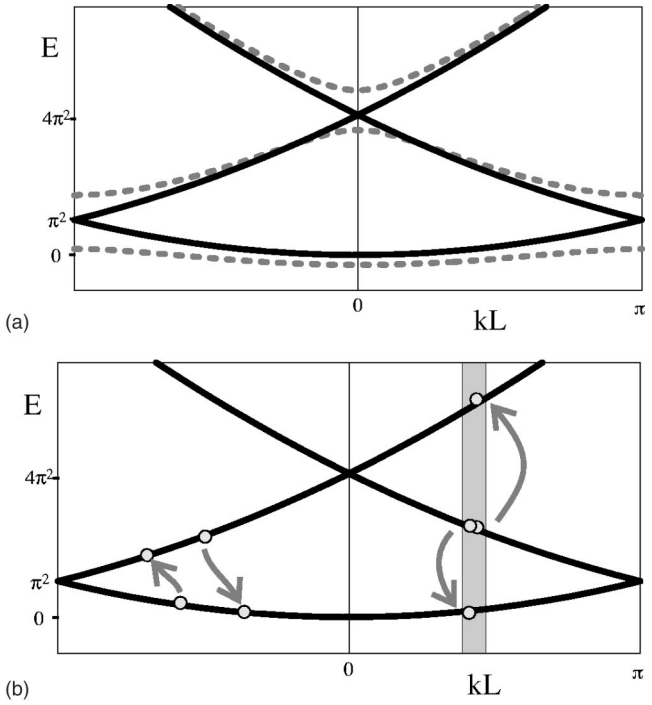

FIG. 10. Illustration of the terms in Hamiltonian (5). In (a), the black line shows the kinetic energy $H_{\rm kin}$ of single-particle states as a function of crystal momentum k. The periodic potential $H_{\rm pot}$ couples states with the same k, splitting the degeneracies, giving rise to the band structure shown as a dotted gray line. In (b) scattering processes are illustrated. On the left-hand side a generic scattering event is shown where two particles with arbitrary momenta, scatter to two other states. On the right a ''vertical'' scattering event is shown, where two particles with the same crystal momentum scatter to two other states, preserving k. These vertical scatterings are included in $H_{\rm int}^{\rm (vert)}$, while all others are in $H'_{\rm int}$. Energies are measured in units of $\hbar^2/2mL^2$.

In our subsequent analysis we will ignore $H'_{\rm int}$. This is a quite drastic approximation which clearly restricts the phenomena which can be studied. For example, the superfluid-insulator transition seen in Ref. [13] cannot be studied in this model. However, all studies of atoms in optical lattices which rely upon mean-field theory (the Gross-Pitaevskii equation) implicitly make this truncation whenever they limit themselves to a Bloch ansatz [22]. This approximation therefore has a range of validity which is a superset of the mean-field theory's. In particular, this approximation is good when the interaction strength is the smallest energy in the problem.

Once $H'_{\rm int}$ is eliminated, the sectors of different k are independent. If one identifies k with the Φ in Eq. (2), then the two Hamiltonians are identical. For the remainder of the paper, we work with Eq. (2), while keeping in mind that all results can also be applied to a gas of particles in a periodic lattice.

III. ENERGY LANDSCAPE IN ABSENCE OF IMPURITY

Here, and in the following section, we calculate the properties of the microscopic model (2), finding the general struc-

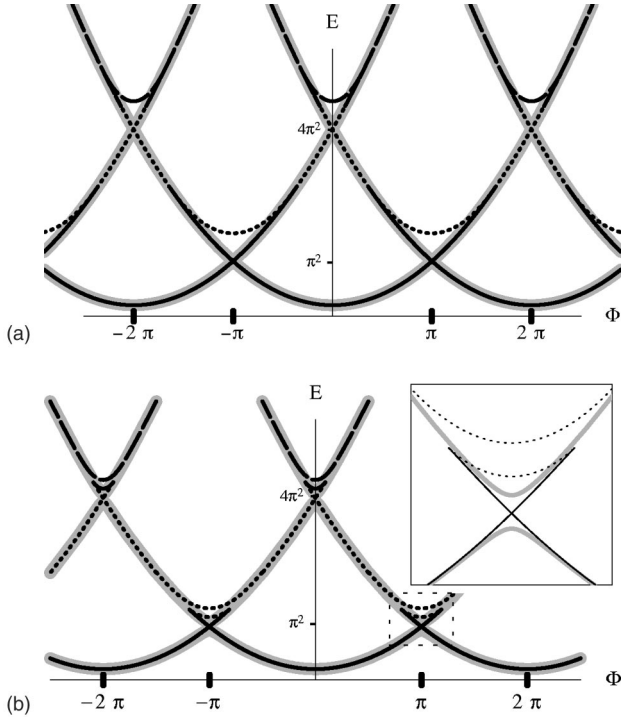

FIG. 11. Spectra. Thick gray lines, single-particle energy levels of noninteracting particles in a 1D ring of length L. Black lines, mean-field energy extrema of interacting system, with global mean-field shift removed. Solid lines are local minima, dotted (dashed) lines are saddle points/cusps with one (two) direction of negative curvature/slope. (a) and (b) are, respectively, with and without an added impurity. In (b) the area around $\Phi=\pi$ is enlarged and displayed in an inset. Energies are measured in units of $\hbar^2/2mL^2$. Notice the similarities between the single-particle states for particles in the ring shown here, and the band structure for particles in a periodic potential in Fig. 10.

tures discussed in the introductory sections. We divide the discussion into several sections, based upon the limits of various parameters and the mathematical techniques used.

A. Two-mode approximation

It is instructive to first analyze Eq. (2) in the absence of an impurity, and in the limit where the interactions are sufficiently weak, i.e., where $\lambda=0$ and $gN\ll 1$, with N being the number of particles. The noninteracting single-particle energy states are shown as thick gray lines in Fig. 11 as a function of Φ. This spectrum and the physical properties that we are interested in are periodic in Φ, and it suffices to consider $-\pi\leqslant\Phi\leqslant\pi$. The ground state, in the absence of interactions, consists of all particles condensed in the lowest-energy state. Aside from providing a global shift in the chemical potential, weak interactions only introduce a significant perturbation when the energy difference between two levels is less than $gN/2$, so that the interactions mix the two states. Focusing on the level crossing at $\Phi=\pi$, the system is reduced to two levels with an effective Hamiltonian,

$$H_\pi=(\phi+\pi)^2 n_0+(\phi-\pi)^2 n_1+\frac{g}{2}(n_0^2+n_1^2+4n_0n_1), \tag{11}$$

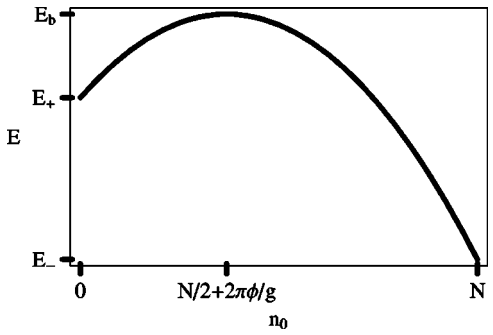

FIG. 12. Energy barrier separating persistent current carrying states within the two-mode approximation. The ordinate shows n_0, the number of particles in the $l=0$ state, the remaining $N-n_0$ particles are in the $l=1$ state. The maximum occurs at $n_0=\overline{n_0}=N/2+2\pi\phi/g$, where ϕ is a measure of the rotation speed, and g the interaction strength. A barrier only exists when $0<\overline{n_0}>N$. The labeled energies E_b and $E_\pm$ are given in the text.

where $\phi=\Phi-\pi$, and $n_j=c_j^\dagger c_j$ are constants of motion. The eigenstates $|n_0,n_1\rangle=(c_0^\dagger)^{n_0}(c_1^\dagger)^{n_1}|0\rangle/\sqrt{n_0!n_1!}$, have a fixed number of particles in each momentum state. Just like in the noninteracting system, for $\phi<0$ ($\phi>0$) the ground state is $|N,0\rangle$ ($|0,N\rangle$). Interactions play a role here only through the fact that when $\gamma=2\pi|\phi|/g<N/2$ a barrier, as illustrated in Fig. 12, separates these two states. This barrier exists because density modulations are required to transfer particles between angular momentum states. In the presence of interactions these modulations cost energy. The barrier state, $|N/2+\gamma,N/2-\gamma\rangle$, has energy $E_b=(\phi+\pi)^2(N/2+\gamma)+(\phi-\pi)^2(N/2-\gamma)+3gN^2/4-g\gamma^2$, compared to $E_\pm=(\phi\pm\pi)^2N+gN^2/2$ for the other extrema. The maximum barrier height (occurring at $\phi=0$) is $\delta E=gN^2/4$.

This same scenario is repeated at all other level crossings in Fig. 11. Thus, in this weakly interacting limit, one can take the eigenstates of Eq. (2) to be the ''Fock'' states

$$|n_0,n_1,n_{-1},\ldots\rangle=\prod_j\frac{(c_j^\dagger)^{n_j}}{\sqrt{n_j!}}|0\rangle, \tag{12}$$

where the occupation numbers n_j obey the constraints $n_j>0$ and $\Sigma_j n_j=N$. For large numbers of particles there is no approximation involved in thinking of the n_j as continuous variables.

We have already detailed the energy landscape when we truncate this space to two n_j's, and the space of allowed states consists of a line (the x axis of the plot in Fig. 12). When three n_j's are included, the space is a triangle, and with four n_j's it is a tetrahedron. The d-dimensional generalization of a triangle/tetrahedron is often called a simplex or a hypertriangle, and within our approximations, the eigenstates of the Hamiltonian form an infinite-dimensional simplex. The corners of this simplex are cusps in the energy topography. Cusps play a role similar to saddle points, as they are each classified by the number of independent directions in which the energy decreases.

As explicitly shown in Fig. 12 for the case of two levels, there exists a range of Φ for which one can find extrema in

addition to these cusps. In Fig. 11, the extrema are marked by the number of ''downward'' directions. Loops are clearly visible around points where the noninteracting states cross. These loops get smaller when the interaction strength decreases. Taking g and Φ as the control parameters, one reproduces the structure in Fig. 3.

As in our generic discussion, these loops lead to hysteresis. Suppose our model one-dimensional (1D) gas starts in the state $|N,0\rangle$ at $\Phi=0$, and is then accelerated so that Φ is slightly larger than π. The barrier will then keep the system from jumping into the new ground state $|0,N\rangle$. Thus the presence of this barrier implies the existence of persistent currents. Of course, since we have considered only very small interactions, these currents only exist near $\Phi=\pm\pi$.

B. Mean-field theory

A useful tool to further illucidate our model (2) is mean-field theory. Here we use a mean-field theory to show that the general structure of metastability and superfluidity found within the two-mode approximation continues to be valid for larger interaction strengths.

This discussion reveals several important points.

(1) Even though a one-dimensional Bose gas is a Luttinger liquid and is usually not studied using mean-field theory, we show below that *mean-field theory correctly describes the behavior of a one-dimensional Bose gas for a significant parameter range*. The exact details of this parameter range is discussed below.

(2) The extrema of the mean-field Hamiltonian are in one-to-one correspondence with the energy extrema in the many-body Hilbert space discussed in Sec. III A.

(3) In the regime where both the two-mode approximation and mean-field theory are applicable, the Bogoliubov excitation spectrum of the mean field coincides with the exact low-energy excitations of the many-body problem. This correspondence is well known from the Bethe ansatz analysis of the one-dimensional Bose gas [20].

1. The two-mode regime

We begin by considering mean-field theory in the regime where the two-mode approximation is valid. For weakly interacting Bosons, mean-field theory can be formulated as a variational method in which one assumes that all of the particles are in the same single-particle state. In the effective two-level Hilbert space described by the Hamiltonian in Eq. (11), we consider wave functions of the form $|\alpha,\beta\rangle=(\alpha a_0^\dagger+\beta a_1^\dagger)^N|0\rangle$, where the variational parameters α and β satisfy $|\alpha|^2+|\beta|^2=1$, and $|0\rangle$ is the vacuum state containing no particles. For $\phi<0$ ($\phi>0$), the energy is minimized by $|\alpha|^2=1$, $|\beta|^2=0$ ($|\alpha|^2=0,|\beta|^2=1$), which (within the two-mode approximation) is the exact ground state as shown in Sec. III A. When $|\phi|<g(N-1)/4\pi$, one also finds a mean-field state which is a maximum of the energy, corresponding to the barrier state found previously. The topography of the mean-field energy landscape mirrors that of the exact eigenstates, and the barriers found within the mean-field theory do not differ significantly from the exact barriers.

It is quite striking that the mean-field theory compares so favorably with the exact two-mode calculation, considering that the exact barrier state contains two, rather than one, condensates and is therefore referred to as ''fragmented'' [23]. The connection between these states is understood by noting that that the mean-field barrier corresponds to a ''phase slip,'' where the fluid density vanishes at some point. By its nature, such an event breaks rotational symmetry. Averaging over the possible location of the slip restores the broken symmetry, and leads to the exact (fragmented) barrier state [24].

In this weakly interacting limit the excitations of the mean-field theory correspond to the exact low-lying excited states of the two-mode system. This result is trivially obtained by substituting our variational wave function into Eq. (11) and calculating the frequencies of small oscillations. For those familiar with dilute gases of bosons, this result is perhaps even simpler to derive by going beyond the two-mode approximation, and directly writing down the excitations of a condensate moving at velocity v_c. As with a three-dimensional system, an excitation of wave vector k is given by the Bogoliubov form,

$$E_k=\frac{\hbar^2}{2m}\sqrt{k^2(k^2+2gN/L^2)}-v_c k. \tag{13}$$

Here the finite size of the ring restricts the wave vector to $k=2\pi n/L$, with integer n. Similarly $v_c=2\pi\hbar n'/(mL)$ is quantized with integer n'. In the frame rotating with velocity Ω the excitations have energies $E_k-\hbar\Omega L/2\pi$. Within the two-mode approximation we are limited to $n=1$, and it is straightforward to verify that excitation spectrum matches the low-energy spectrum calculated directly from Eq. (11). Exploring the excitation spectrum around the saddle-point state, one finds a zero-mode corresponding to translations of the phase slip, and negative-energy modes corresponding to falling towards one of the local minima. In the exact two-mode theory, the zero mode corresponds to changing the relative phase between the modes.

2. Beyond two modes

In addition to the insights provided above, the mean-field approach also provides a systematic way to explore Eq. (2) for interaction strengths that are beyond the scope of the two-mode approximation. The mean-field theory involves replacing the field operators c_k with c numbers. It is convenient to work in real space, defining a ''condensate wave function'' $\psi(x)$ by

$$c_k=\int_0^1 dx e^{ikx}\psi(x), \tag{14}$$

where $\int dx|\psi(x)|^2=N$, is the number of particles. An energy landscape can be found in the space of all possible square integrable complex-valued functions $\psi(x)$. This landscape contains all of the structures seen in the two-mode version of mean-field theory. In particular, the $k=n$ states given by $\psi_n(x)=\sqrt{N}e^{i2nx}$, are always stationary points. Their stability is given by the Landau criterion that if the excitation spec-

trum in Eq. (13) is positive then they are local minima. Otherwise there exists a direction of negative curvature. The existence of multiple minima in the energy landscape leads to hysteresis and superfluidity.

When both the $k=n$ and $k=n-1$ states are locally stable, there must exist a saddle point separating them. As in the two-mode case this saddle point involves a ''phase slip,'' where the density vanishes and the number of units of circulation can change. The real space wave function of the phase slip takes on the form of a hyperbolic trigonometric function, whose exact form was determined by Langer and Ambegaokar in the context of superconductors [25]. The barrier height is understood by recognizing that the length scale for the phase slip is the healing length ξ ($\approx 1/\sqrt{gN}$ in our dimensionless units). The presence of the slip increases the density from N to $N/(1-\xi)$, at an energy cost per particle of $gN\xi \rightarrow \hbar^2\sqrt{a_s L/d_\perp^2}/mL^2$ in physical units (assuming transverse harmonic confinement with length scale $d_\perp = \sqrt{\hbar/m\omega}$). A more careful calculation, detailed in Ref. [26], verifies this result with a coefficient $\sqrt{32/9}$.

3. Limits of validity

We have shown that within mean-field theory the one-dimensional Bose gas is superfluid in that it exhibits hysteresis under changing the rotation speed. It is therefore very important to understand the limits of validity of mean-field theory. We estimate these limits by calculating the depletion within a Bogoliubov approach (for example, see Ref. [27]), where one finds that

$$\frac{\delta N}{N} = \sum_k \frac{\epsilon_k - E_k}{2E_k} \sim \sqrt{\frac{g}{N}} \ln(gN), \tag{15}$$

where $\epsilon_k = \hbar^2/2m(k^2 + gN/L^2)$. Only when this ratio is small compared to 1 is the mean-field theory valid. For experimentally relevant parameters, the logarithm is of order ten, and the prefactor $\sqrt{g/N}$ determines the size of the depletion. A physical interpretation of this factor is that the healing length ξ ($1/\sqrt{gN}$) which governs the scale of the phase slip must be larger than the interparticle spacing ($1/N$) for fluctuations to be small and for mean-field theory to be applicable (i.e., phase slips cost very little energy if they fit between particles). To study stronger interactions one needs to include short-range fluctuations—either through ''bosonizing'' the system [19], or by using the Bethe ansatz [20].

Substituting plausible experimental values into Eq. (15) shows that it is much easier to be in the regime where mean-field theory is applicable than it is to be in the strongly correlated regime. For example, with 10^6 atoms of ^{87}Rb (with scattering length $a_s \approx 5$ nm) in a ring of circumference $L = 100\ \mu$m, and transverse confinement $\omega_\perp = 500\ \mathrm{s}^{-1}$ (corresponding to $d_\perp \sim 1\ \mu$m) one finds $\delta N/N \sim 0.2\%$. Decreasing N or increasing L leads to proportionally more depletion and can bring one into the strongly correlated regime.

IV. PERSISTENT CURRENTS IN THE PRESENCE OF IMPURITY

Having established the superfluid behavior of a weakly interacting gas through analysis of the energy landscape, we now analyze the behavior of such a system when a small impurity is added. We shall see that as long as the impurity strength is small compared to the interactions, such an impurity leads to extremely slow (typically exponentially slow) decay of persistent currents. In the opposite limit, where the impurity is strong, no persistent currents nor hysteresis exists.

Even when the impurity is weak, it does have a dramatic effect on the (mean-field) energy landscape in Fig. 11, in that it opens up gaps as seen in Fig. 11(b). In the case of atoms in a periodic potential these gaps are the familiar band gaps from solid-state physics discussed in the Introduction. Note that the gaps do not change the fact that one has hysteretic behavior signaled by the swallow-tail loops. In this section we present the quantitative theory of these loops in the limit of weak interactions and calculate the quantum tunneling from one local minimum to another (i.e., the decay of persistent currents induced by quantum fluctuations).

A. Two-mode model

Interactions are most easily understood within a two-mode model. For its validity we will need both weak interactions $gN \ll 1$, and a weak impurity $\lambda \ll 1$. The ratio λ/gN which compares the impurity strength to the interaction strength is arbitrary. As before, it suffices to consider the system near $\phi = \Phi - \pi = 0$, where the Hamiltonian may be truncated to Eq. (11), with an additional impurity term $H_{\mathrm{imp}} = \lambda(a_1^\dagger a_0 + a_0^\dagger a_1)$. This system of N bosons in two states can be mapped onto the precession of a spin $N/2$ object obeying a Hamiltonian

$$H_{\mathrm{spin}} = 4\pi\phi S_z + 2\lambda S_x - 2gS_z^2 + C_N, \tag{16}$$

where $S_z = (a_0^\dagger a_0 - a_1^\dagger a_1)/2$, $S_x = (S_+ + S_-)/2$, $S_y = (S_+ - S_-)/2i$, $S_+ = a_0^\dagger a_1$, and $S_- = a_1^\dagger a_0$ obey the standard spin algebra, and C_N is an uninteresting c number. This mapping is the inverse of the method of ''Schwinger bosons'' [28]. The quantum dynamics of such large spins are well understood [29], so we only briefly outline the analysis necessary to understand the mean-field structure, and the decay of persistent currents.

The classical (mean-field) energy landscape of the spin is shown in Fig. 13, where the angles θ and ϕ describe the direction in which the ''spin'' is pointing. In the absence of interactions, there are two stationary points, a maximum and a minimum. These represent the first and second band in the single-particle energy spectrum. For sufficiently strong interactions

$$(gN)^{2/3} > (2\pi\phi)^{2/3} + \lambda^{2/3}, \tag{17}$$

a second minimum and a saddle spontaneously appear (a saddle-node bifurcation), giving rise to the swallow-tail energy spectrum shown in Fig. 11. The new minimum is analo-

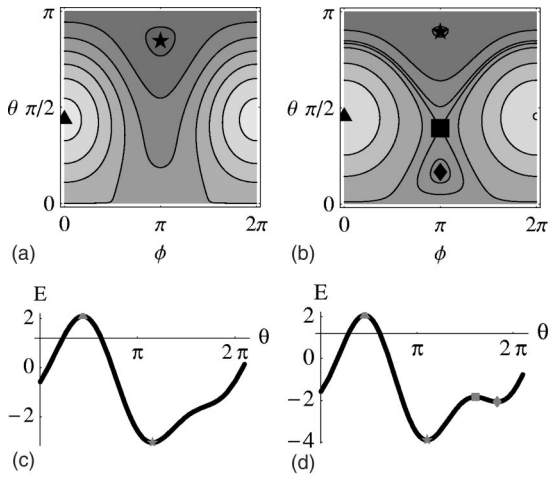

FIG. 13. Energy landscape of spin which represents the state of the one-dimensional Bose gas within a two-mode approximation in the presence of an impurity. The number of particles with angular momentum $l=0$ ($l=\hbar$) is $N\cos^2(\theta)[N\sin^2(\theta)]$, while ϕ is the phase angle describing the coherence between these states. For the contour plots, (a) and (b), darker colors represent lower energy; stars, triangles, diamonds, and squares represent the global minimum, global maximum, local minimum, and saddles. In (a) the inequality in Eq. (17) is not satisfied ($\phi=0.16,\lambda=2,g=3.16$), and only two extrema exist, while in (b) the inequality is satisfied ($\phi=0.16,\lambda=2,g=5.16$). A nonlinear scale is used for the contours in (b) to emphasize the extrema. All of the extrema occur on a great circle parametrized by setting $\phi=0$ and letting θ run from 0 to 2π. This corresponds to a path from the ''south pole'' to the ''north pole'' along the ''meridian'' where $\phi=0$, and returning along the $\phi=\pi$. (c) and (d) show the energies of (a) and (b) as a function of θ along these paths. The structures from Fig. 1 are clearly seen. Energies are measured in units of $\hbar^2/2mL^2$.

gous to the metastable states found in the absence of the impurity. The difference here is that this metastable state is distinct from the upper band, which is still represented by the maximum. In the symmetric case ($\phi=0$), the minima occur at $S_z=N/2\sqrt{1-(\lambda/gN)^2}$, and the barrier has a height $E_b=gN^2/2(1-\lambda/gN)^2$ as is clear from Eq. (17), the metastable state can only exist if the interaction strength gN exceeds the impurity strength λ.

B. Quantum tunneling in the two-mode limit

Quantum mechanically, there are matrix elements for tunneling from the upper minima to the lower, and the upper state acquires a finite lifetime. For those more familiar with particle tunneling than with spin tunneling it may be helpful to instead map the problem onto the motion of a particle on a one-dimensional lattice. Introducing states $|m\rangle=(-1)^m|n_0=N/2+m,n_1=N/2-m\rangle$ and operators $c_m^\dagger$, which create these states, the many-body problem in the two-mode approximation is equivalent to a single particle with a Hamiltonian

$$H=\sum_m \left[(4\pi\phi m - g m^2) c_m^\dagger c_m - \lambda \sqrt{\left(\frac{N}{2}+m+1\right)\left(\frac{N}{2}-m\right)} \times (c_{m+1}^\dagger c_m + c_m^\dagger c_{m+1}) \right] + C_N', \tag{18}$$

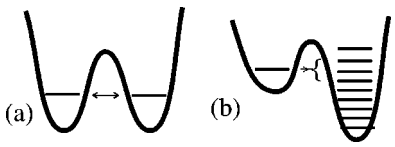

FIG. 14. Schematic representation of tunneling within a double-well system: (a) coherent tunneling between resonant states; (b) incoherent decay from a single state on the left to a large number of states on the right. (Here this decay corresponds to a transition from a current-carrying state to a stationary one with a large number of phonon excitations.)

where C_N' is an uninteresting c number. This Hamiltonian represents a particle on a lattice with an inverted parabolic potential and an unusual spatially dependent hopping (which can be viewed as a spatially dependent mass). A particle surmounting a barrier by hopping on such a discrete lattice behaves somewhat differently than a similar particle with a continuous coordinate. In particular, for sufficiently large barriers, the tunneling rate is a power law in λ rather than the familiar exponential. Such power-law behavior was predicted by Kagan *et al.* in discussing the finite-temperature lifetime of persistent currents [21].

An important conceptual point to consider here is to what extent the scenario discussed so far can lead to the decay of a current. We have reduced the many-body problem to the one-dimensional quantum-mechanical motion of a single particle. There is no source of dissipation within this model, and one would naively expect to see coherent oscillations between the two wells rather than a decay. This intuition is, in fact, correct when the two wells are degenerate (i.e., $\phi=0$), or when the tunneling is extremely weak. This coherent tunneling limit is illustrated in Fig. 14(a), in which only the lowest state in each well is coupled. When there is a significant mismatch in the energies of the two wells, say the left-hand well has more energy than the other, the situation is different. As pictured in Fig. 14(b), the ground state on the left can be coupled to several excited states on the right, a situation analogous to an excited atom coupled to a large number of vacuum modes. In the limit of large N, the spacing between the modes in the right-hand well vanish, and the state on the left-hand side of the barrier acquires a finite lifetime. A detailed study of this crossover from coherent oscillations to decay is found in Ref. [30]. One expects decay whenever the tunneling rate is significantly larger than $\Delta/\hbar$, where Δ is the characteristic energy spacing (here given by the inverse of the density of states of Bogoliubov phonons).

A semiclassical analysis of Eq. (18) is detailed in Ref. [29]. The eigenvalues of Eq. (18) are found by solving a difference equation. This difference equation can be approximated by a differential equation which is amenable to a WKB analysis. The resulting expression for the lifetime τ of the persistent current is

$$\tau=\tau_0 \exp\left(\int_{b_1}^{b_2} \operatorname{arccosh}\frac{-2gs^2+4\pi\phi s-E}{2\lambda\sqrt{(N/2)^2-s^2}} ds \right). \tag{19}$$

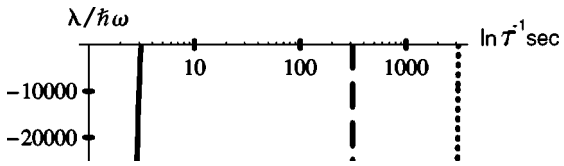

FIG. 15. Lifetime of a metastable current-carrying state (19) in a toroidally trapped Bose gas in the presence of an impurity of strength λ. For this figure, we consider the case where the trap is rotating at exactly one half quantum of circulation $\phi=0$. In the curves shown, the trap is described by a circumference L, a transverse confinement frequency ω, a number of particles N. These are, respectively: solid line, $L=10^{-2}$ m, $N=10^6$, $\omega=500\ \mathrm{s}^{-1}$; dashed line, $L=10^{-4}$ m, $N=10^7$, $\omega=500\ \mathrm{s}^{-1}$; dotted line, $L=10^{-2}$ m, $N=10^8$, $\omega=50\,000\ \mathrm{s}^{-1}$. One expects that imperfections in the apparatus would lead to $\lambda \ll \hbar\omega$. In all cases the particles are taken to have scattering length $a_s=5$ nm and mass $m=85$ a.u. The metastability turns on so quickly that the curves appear nearly vertical, even on this logarithmic scale.

The attempt frequency τ_0^{-1} is roughly the frequency of small oscillations about the local minimum of Eq. (16). This frequency also coincides with the quantum-mechanical energy of excitations in the metastable state (which, as already pointed out, is the energy of Bogoliubov excitations). For the symmetric case, $\phi=0$, one finds $\tau_0^{-1}\sim 2\sqrt{(gN)^2-\lambda^2}$. The integration variable s corresponds to the projection of spin S_z, the limits of integration b_1 and b_2 are the classical turning points, and E is the energy, given by Eq. (16) with the constant C_N removed. When $s=b_{1,2}$ the argument of the arccosh is 1.

For sufficiently small barriers, $E_b \ll \lambda N$, the arccosh can be expanded as $\mathrm{arccosh}(1+x)=\sqrt{2x}+O(x^{3/2})$, yielding a decay rate which is exponentially small in the impurity strength, $\tau^{-1}\sim\exp(-\alpha\sqrt{NE_b/\lambda})$, where α is of order unity. For larger barriers, one can expand $\mathrm{arccosh}(z)=\ln(2z)+O(z^{-2})$, which leads to a power-law behavior, $\tau^{-1}\sim(N\lambda/E_b)^{-\beta E_b/N}$, where $\beta\approx 1$. Unless the barrier is tuned extremely close to zero, both of these expressions yield astronomically large lifetimes whenever a barrier exists. Thus, the condition for superfluidity reduces to the condition for a barrier (17). In Fig. 15, Eq. (19) is numerically integrated for some representative parameters, verifying these asymptotics.

ACKNOWLEDGMENTS

This work was supported by NASA, Grant Nos. NAG8-1441 and NAG8-1765, and by NSF, Grant Nos. DMR-0109255 and DMR-0071630. The author would like to thank Tin-lun Ho for his kind support and insightful suggestions, and both Q. Niu and Mehmet Oktel for critical comments. The use of a two-mode approximation to study superfluidity was first introduced to me by A. J. Leggett in private communications (the two-mode model with $g<0$ is discussed in Ref. [31]).

[1] A. J. Leggett, Rev. Mod. Phys. **73**, 307 (2001).
[2] B. Wu and Q. Niu, Phys. Rev. A **61**, 023402 (2000).
[3] Dmitri Diakonov, L. M. Jensen, C. J. Pethick, and H. Smith, Phys. Rev. A **66**, 013604 (2002).
[4] Much of the study of swallow tails is rooted in the exact solutions to the Gross-Pitaevskii equation derived in, J. C. Bronski, L. D. Carr, B. Deconinck, and J. N. Kutz, Phys. Rev. Lett. **86**, 1402 (2001); J. C. Bronski, L. D. Carr, B. Deconinck, J. N. Kutz, and K. Promislow, Phys. Rev. E **63**, 036612 (2001); J. C. Bronski, L. D. Carr, R. Carretero-González, B. Deconinck, J. N. Kutz, and K. Promislow, *ibid.* **64**, 056615 (2001).
[5] Jie Liu, Libin Fu, Bi-Yiao Ou, Shi-Gang Chen, Dae-Il Choi, Biao Wu, and Qian Niu, Phys. Rev. A **66**, 023404 (2002).
[6] L. D. Landau and E. M. Lifshitz, *Statistical Physics Part 1* (Pergamon, New York, 1980).
[7] R. Thom, *Structural Stability and Morphogenesis* (Benjamin, Reading, Massachusetts, 1975).
[8] The hypothetical experiment discussed here is an amalgam of W. F. Vinen, Proc. R. Soc. London, Ser. A **260**, 218 (1961); S. C. Whitmore and W. Zimmermann, Phys. Rev. **166**, 181 (1968); P. W. Karn, D. R. Starks, and W. Zimmermann, Phys. Rev. B **21**, 1797 (1980).
[9] See A. J. Leggett, J. Stat. Phys. **93**, 927 (1998); Rev. Mod. Phys. **71**, S318 (1999), for a detailed discussion.
[10] R. P. Feynman, *Statistical Mechanics* (Addison-Wesley, Reading, 1972), Chap. 11.
[11] Mark Raizen, Christophe Salomon, and Qian Niu, Phys. Today **50**, 30 (1997).
[12] D. Choi and Q. Niu, Phys. Rev. Lett. **82**, 2022 (1999).
[13] Markus Greiner, Olaf Mandel, Tilman Esslinger, Theodor W. Hänsch, and Imamanuel Bloch, Nature (London) **415**, 39 (2002).
[14] Neil W. Ashcroft and N. David Mermin, *Solid State Physics* (Sanders College, Fort Worth, 1976).
[15] Biao Wu, R. B. Diener, and Qian Niu, Phys. Rev. A **65**, 025601 (2002).
[16] M. R. Andrews, D. M. Kurn, H.-J. Miesner, D. S. Durfee, C. G. Townsend, S. Inouye, and W. Ketterle, Phys. Rev. Lett. **79**, 553 (1997); **80**, 2967 (1998).
[17] A lucid discussion can be found in Ref. [1], p. 336. Also see references therein.
[18] J. A. Sauer, M. D. Barrett, and M. S. Chapman, Phys. Rev. Lett. **87**, 270401 (2001).
[19] F. D. M. Haldane, Phys. Rev. Lett. **47**, 1840 (1981).
[20] Elliot H. Lieb and Werner Liniger, Phys. Rev. **130**, 1605 (1963); Elliot H. Lieb, *ibid.* **130**, 1616 (1963).
[21] Yu. Kagan, N. V. Prokof'ev, and B. V. Svistunov, Phys. Rev. A **61**, 045601 (2000).
[22] The mean-field studies of Wu *et al.* [2,12], relax the Bloch ansatz to calculate the stability of the mean-field state. Their analysis can be reproduced by perturbatively including H'_{int}.
[23] P. Nozieres and D. Saint James, J. Phys. (Paris) **43**, 1133 (1982).
[24] Erich J. Mueller, Gordon Baym, Tin-Lun Ho, and Masahito Ueda (unpublished).
[25] J. Langer and V. Ambegaokar, Phys. Rev. **164**, 498 (1967).

[26] Erich J. Mueller, Paul M. Goldbart, and Yuli Lyanda-Geller, Phys. Rev. A **57**, R1505 (1998).
[27] Alexander L. Fetter and John D. Walecka, *Quantum Theory of Many-Particle Systems* (McGraw-Hill, San Francisco, 1971).
[28] See, J. J. Sakurai, *Modern Quantum Mechanics* (Addison-Wesley, Reading, 1994), p. 217.
[29] J. L. Van Hemmen and A. Sütö, Physica B & C **141**, 37 (1986).
[30] V. A. Benderskii and E. I. Kats, Phys. Rev. E **65**, 036217 (2001).
[31] Masahito Ueda and Anthony J. Leggett, Phys. Rev. Lett. **83**, 1489 (1999).